Directing transformation pathways of hierarchical assemblies by recycling oxidative photolysis

Patrick Roth[Δ,1], Raphael Meyer[Δ,1], Manfred Wagner[1], David Y. W. Ng[1]*, Tanja Weil[1]*

[1]Max Planck Institute for Polymer Research, Ackermannweg 10, 55128 Mainz, Germany

Email Correspondence: david.ng@mpip-mainz.mpg.de, weil@mpip-mainz.mpg.de

[Δ]Represents Equal Contribution

Keywords: peptide, self-assembly, structural plasticity, systems chemistry, complex reaction networks

Abstract

Structure formation in living systems builds upon balancing kinetic and thermodynamic landscapes powered by recycling covalent bond chemistry. Although recent synthetic efforts have been able to achieve these processes in part, the combination is necessary to identify key mechanisms that confer nature's structural precision within a complex environment. We design a photolytic peptide that dissipates downstream chemical energy to control the transience and interconversion between its two active supramolecular forms via disulfide formation. The thiol assembles with slow kinetics via an isodesmic mechanism whereas the disulfide form induces aromatic chirality that propagates into helical twists within the nanostructure. Multiple structural states found under the same global conditions show that the assembly network demonstrate similar biological plasticity and can be directed by the recycling pathway. The approach demonstrate the importance of reaction complexity in creating supramolecular architectures that are inaccessible via conventional means.

Introduction

The recycling of chemical energy in reaction by-products to direct propagating supramolecular structures is a core feature in complex cellular networks.[1–3] The citric acid cycle in cells produces nucleotide phosphates such as NADH or guanosine-5'-triphosphate (GTP) as by-products when citrate undergoes backbone and functional group transformations into oxaloacetate.[4,5] These high-energy nucleotide phosphates promote, *via* covalent bond formation, the transformation of dormant molecules into active precursors that drive reversible superstructures of cytoskeletal polymers such as actin filaments and microtubules.[6–8] By creating many such connections between reaction

networks, biology not only makes maximum use of chemical energy, but also exerts regulatory control over metabolic pathways across different length scales.[9] Recent efforts have emulated the basics using synthetic small molecules in reversible reaction sequences and have shown that dissipative systems that resemble cellular homeostasis can be created.[10–19]

However, advancing these synthetic systems is a grand challenge because the role of the covalently-bound nucleotide phosphates in cells goes beyond controlling the association rates of polymeric subunits. They also modulate polymer dynamics through structural plasticity, which reflects changes in the structural state of a cytoskeletal polymer without affecting the chemical state of its bound nucleotide.[20] Within the monomer, there exists a conformational switch of the subunits where structural distortion can be initiated to cause a propagative crack axis that tips the favour towards depolymerization. Together, these interactions dictate the ebb and flow of the filamentous assembly, demonstrating how the routing of simple energy-rich molecules can program complex supramolecular behaviour.[21,22]

Within synthetic chemistry, protecting groups constitute a major loss of chemical energy that is typically wasted in a synthesis route once it is cleaved from the molecule of interest.[23] We propose that these deprotected by-products can be recycled in situ, like in biology, to perform covalent transformation that regulates reversible supramolecular assembly. To demonstrate this concept, we take a commonly known photo-protecting group (PPG), 2-nitroveratryloxycarbonyl (nvoc), where the mechanism of photolysis and broad substrate capacity is well established.[24] The nvoc group absorbs UV light (365 nm) to form a zwitterionic excited state followed by an $N{=}O_{nitro}$ bond scission and, upon the expulsion of CO_2, forms a nitrosobenzaldehyde by-product.[24] Aromatic $N{=}O_{nitroso}$ compounds can oxidize thiols into disulfides *via* sequential addition and elimination steps.[25] By combining both reactions, we propose that thiol containing molecules protected with the nvoc group would undergo a recycling transformation into disulfides *in situ*. If the thiol and its disulfide counterpart exhibit different self-assembling features, the kinetics and reversibility of their covalent transformation would ultimately dictate the dynamics, stability and morphology of the formed superstructures.

Herein, we design *iso*(Fmoc-I)nvocCA **1a**, consisting of a masked cysteine connected *via* an thioester to form an isomerized backbone that temporarily blocks self-assembly. The nvoc group is installed at the *N*-terminus of Cys, thus regulating both the isomerization and oxidation recycling. At the molecular level, the reaction sequence is first activated by 365 nm UV irradiation, which cleaves the nvoc group. While the nvoc undergoes a Norrish Type II reaction to form the nitrosobenzaldehyde

group, the peptide performs an *S*,*N*-acyl rearrangement aligning the backbone and thus liberating the Cys-SH group yielding Fmoc-ICA (**3a$^{\lambda}$, Figure 1**).[24] The nitrosobenzaldehyde-containing by-product enters the reaction sequence, oxidizing the free thiol of Fmoc-ICA **3a$^{\lambda}$** into its disulfide form DiFmoc-ICA (**4a$^{\lambda}$**). To provide clarity of the nomenclature, products formed within the recycling cascade denoted as **3a$^{\lambda}$** for Fmoc-ICA and **4a$^{\lambda}$** for DiFmoc-ICA, whereas the independently synthesized control peptides are termed **3a** and **4a**, respectively. Depending on the competing kinetics of supramolecular assembly between **3a$^{\lambda}$** and **4a$^{\lambda}$** against the global chemical energy availability (N=$O_{nitroso}$: dithiothreitol), we can manipulate the transience of **3a$^{\lambda}$** to direct structure propagation, plasticity, supramolecular chirality and polymerization/depolymerisation kinetics. In doing so, we have designed regulatory reaction networks that control the dynamics and complexity of supramolecular nanostructures.

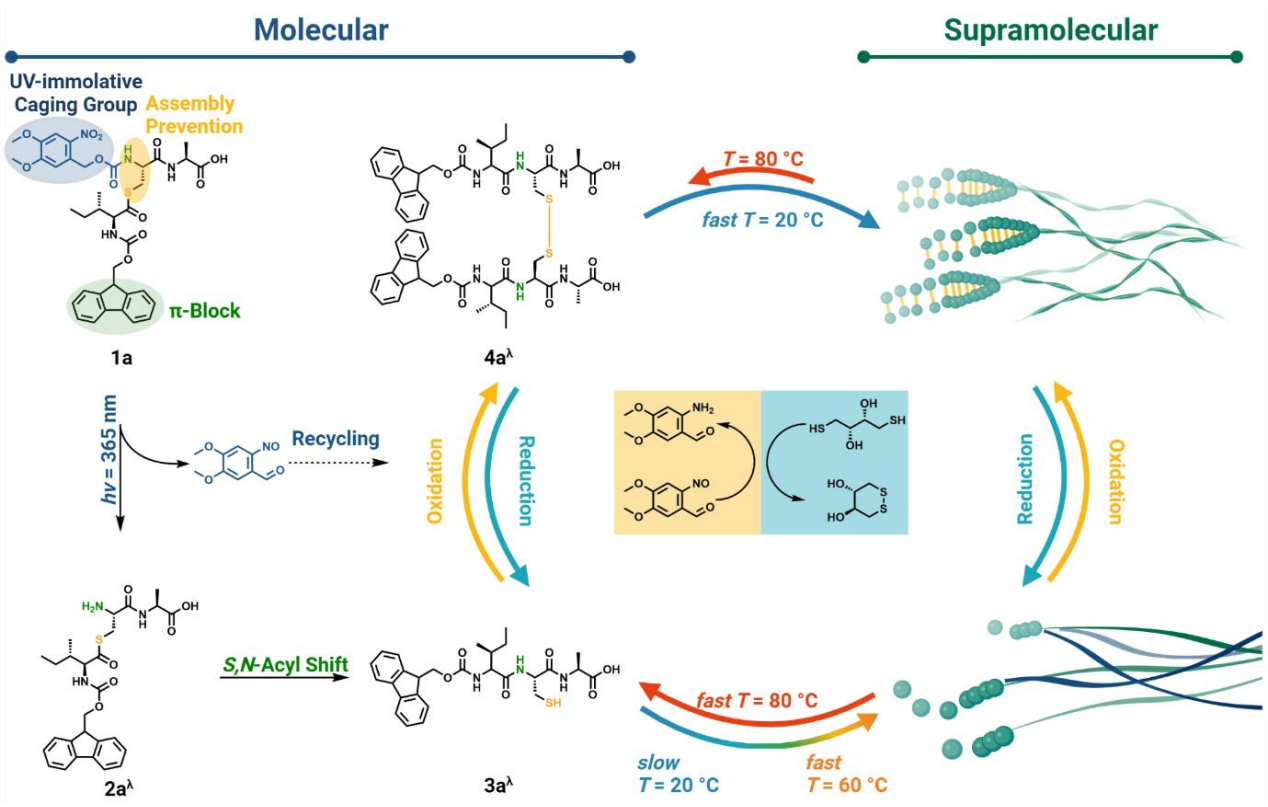

Figure 1. Autonomous reaction pathway of the self-fuelled generation of different dynamic supramolecular nanostructures with characteristic assembly and disassembly kinetics. *Iso*(Fmoc-I)nvocCA **1a** after UV-irradiation (365 nm). Chemical reaction pathway of **1a** after UV-irradiation leading to the decaged *iso*-peptide **2a$^{\lambda}$**, rearrangement/linearization and oxidation of the thiol **3a$^{\lambda}$** to the disulfide **4a$^{\lambda}$**. The nvoc protecting group is recycled as the oxidant to form disulfides and can be delayed by dithiothreitol (DTT). Interconversion

between molecular and supramolecular structures is regulated by competing redox processes and temperature-dependent assembly and disassembly kinetics.

Results and Discussion

Peptide synthesis was carried out using Fmoc solid-phase peptide synthesis on Wang resin using *N,N'*-di*iso*propylcarbodiimide (DIC) and ethyl (2*Z*)-2-cyano-2-(hydroxyimino)acetate (OxymaPure) for the iterative coupling steps (**Figure 2**). To construct an isomerized Cys backbone, Fmoc-cysteine-monomethoxytrityl (Fmoc-Cys(Mmt)-OH) was used to enable orthogonal installation of the nvoc group *via* 6-nitroveratryl chloroformate on the *N*-terminus and the Steglich-esterification at the *S*-terminus. The so-called *iso*-peptide was cleaved off from the resin with trifluoroacetic acid and purified *via* high-performance liquid chromatography (HPLC) to afford **1a**. As reference compounds, Fmoc-ICA **3a**, DiFmoc-ICA **4a** were synthesized using modified protocols (see Supporting Information). The serine analogue, where the cysteine of **1a** is substituted by serine to form **1b**, was also synthesized to elucidate the role of the thiol group in the oxidation step and structural plasticity at the supramolecular level.

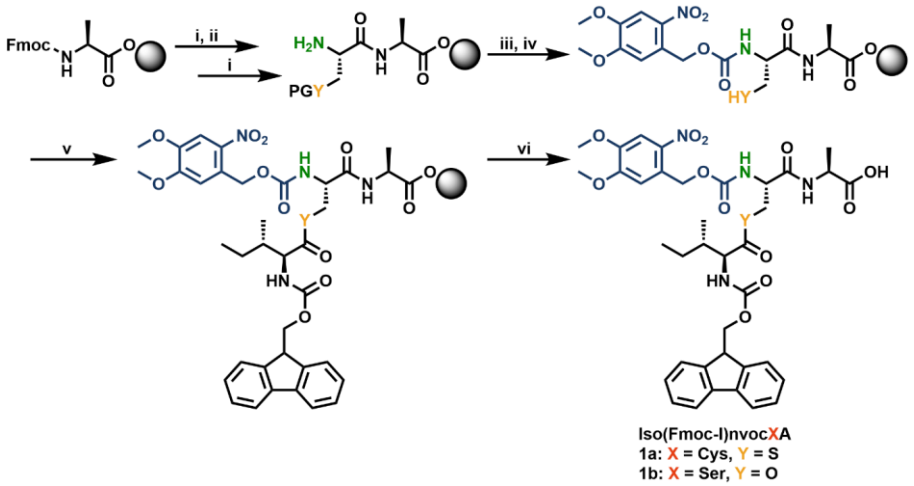

Figure 2: Solid phase synthesis of the *iso*-peptide derivatives. Synthesis of *iso*(Fmoc-I)nvocXA by solid-phase peptide synthesis. (i) Piperidine, (ii) Fmoc-X(PG)-OH, DIC, Oxyma, (iii) NVOC-Cl, TEA, (iv) DCM, TIPS, TFA, (v) Fmoc-Ile-OH, DIC, DMAP, (vi) TFA, TIPS, H_2O.

The recycling cascade was followed by liquid chromatography-mass spectrometry (LC-MS) beginning with a solution of **1a** in MeOH : NH_4HCO_3 buffer (1 : 1) at pH 7.4 (**Figure 3a**). The UV irradiation (365 nm) time was optimized to be 90 s for a deprotection conversion of 94% (**SI Fig. 22**). Upon irradiation, the formation of each intermediate, the deprotected *iso*-peptide **2a$^{\lambda}$**, the *S*,*N*-rearranged peptide **3a$^{\lambda}$** and the oxidation to the disulfide **4a$^{\lambda}$** was monitored over 24 h (**Figure 3b**). Separately synthesized **3a** and **4a** were used as references for the observed retention times. From the kinetics study, the *S*,*N*-acyl shift to **3a$^{\lambda}$** began immediately upon successful deprotection after 2 h. In comparison to the *O*,*N*-acyl shift[26] from **2b$^{\lambda}$** to **3b$^{\lambda}$** depicted in **Figure 3a**, which took up to 72 h to attain a similar conversion (**Figure 3c**), the thiolate demonstrated to be a better leaving group and therefore exhibits an accelerated kinetic profile (**Figure 3e**). Additionally, **3b$^{\lambda}$** is incapable of undergoing further oxidation by the $N{=}O_{nitroso}$ released from the nvoc group. In contrast, oxidation of **3a$^{\lambda}$** into **4a$^{\lambda}$** started after 20 minutes and completion was observed at 24 h (**Figure 3d**).

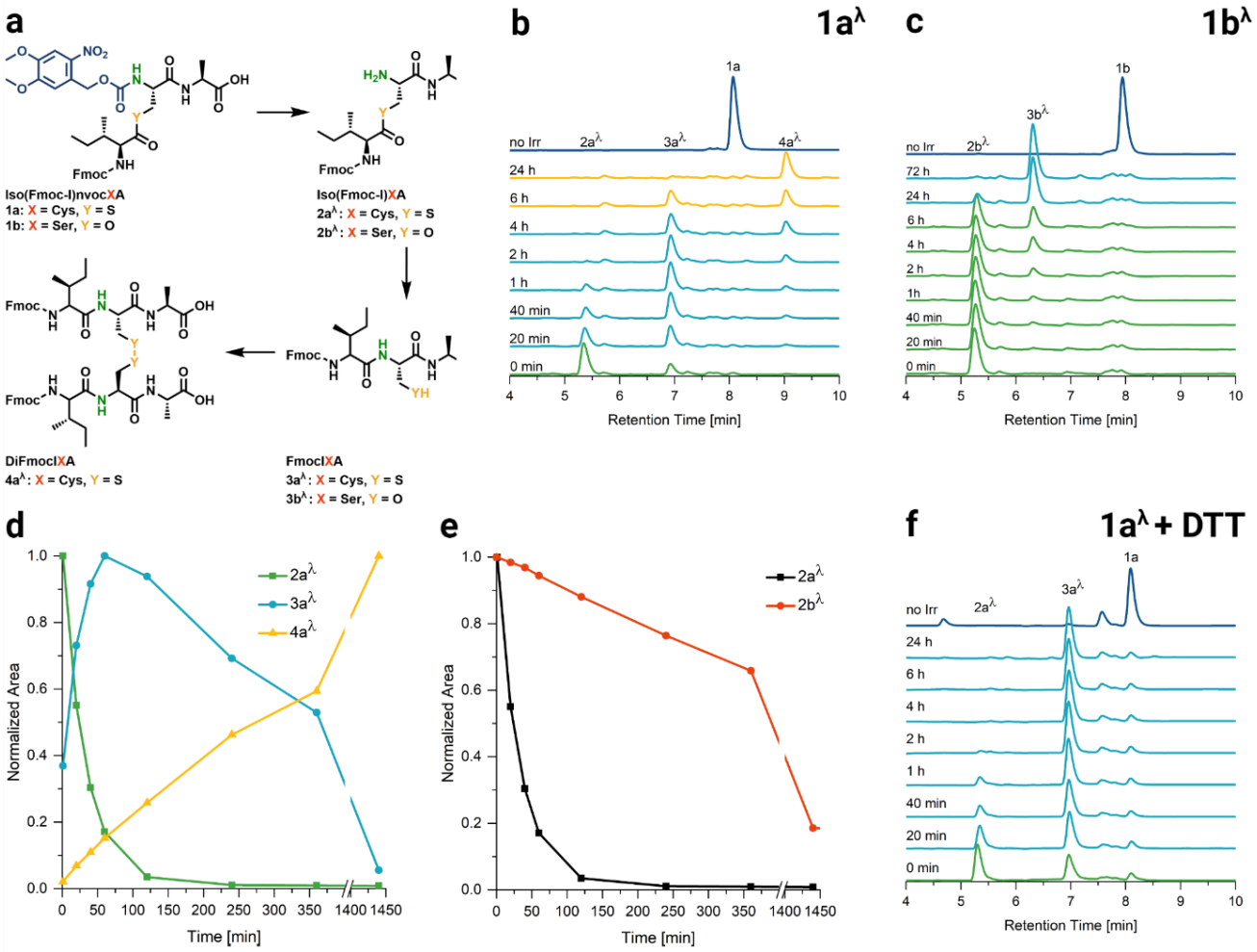

Figure 3. Kinetic profile of *iso*(Fmoc-I)nvocXA derivatives showing accelerated conversion for 1a and recycling pathway. (**a**) Reaction pathway of the two *iso*-peptides after irradiation. (**b**) LC-MS kinetic of *iso*(Fmoc-I)nvocCA (1a) over the time span of 24 h after irradiation. After deprotection, *iso*(Fmoc-I)CA **2a$^{\lambda}$** rearranges into the linear peptide Fmoc-ICA **3a$^{\lambda}$** and oxidizes into the dimer DiFmoc-ICA **4a$^{\lambda}$**. (**c**) LC-MS kinetic of *Iso*(Fmoc-I)nvocSA **1b** over the time span of 72 h after irradiation. After deprotection, *iso*(Fmoc-I)SA **2b$^{\lambda}$** rearranges into the linear peptide Fmoc-ISA **3b$^{\lambda}$**. (**d**) Normalized areas of the intermediates and the product showing relative concentrations over time (**1a$^{\lambda}$**). (**e**) Normalized area of **2a$^{\lambda}$** and **2b$^{\lambda}$** in comparison displaying the differences in reaction kinetics. (**f**) LC-MS kinetic of *iso*(Fmoc-I)nvocCA **1a** 100 µM irradiated with DTT 10 mM.

A control reaction with **3a** revealed that it remained in the reduced form for 24 h under ambient conditions without dimerization, confirming that the oxidation into **4a$^{\lambda}$** was the result of the recycling step by the N=O$_{nitroso}$ by-product of the nvoc group (**SI Fig. 27**). The mechanism was further investigated by using **3a** in the presence of nvoc-Glycine (**5**) to probe whether it is necessary for the nvoc group to be on the same molecule as **3a**. The successful formation of **4a$^{\lambda}$** after irradiation

confirms that the photolysis step first releases the N=O$_{nitroso}$ into the bulk solution and the subsequent oxidation happens in an intermolecular fashion (**Figure 4a**, **SI Fig. 25**). The control over the extent of oxidative recycling can be manipulated in situ with the reducing agent DTT to capture the N=O$_{nitroso}$. Varying amounts of added DTT (5 equiv., 10 equiv., and 100 equiv.) demonstrated time-dependent suppression of the N=O$_{nitroso}$ promoted oxidation, delaying the conversion from **3a$^{\lambda}$** to **4a$^{\lambda}$** (**Figure 4b**). The time delay window is increased by 2 h, 6 h and to >24 h with 5 equiv., 10 equiv. and 100 equiv. of DTT, respectively. This enables the manipulation of the transience of **3a$^{\lambda}$** within the reaction cycle.

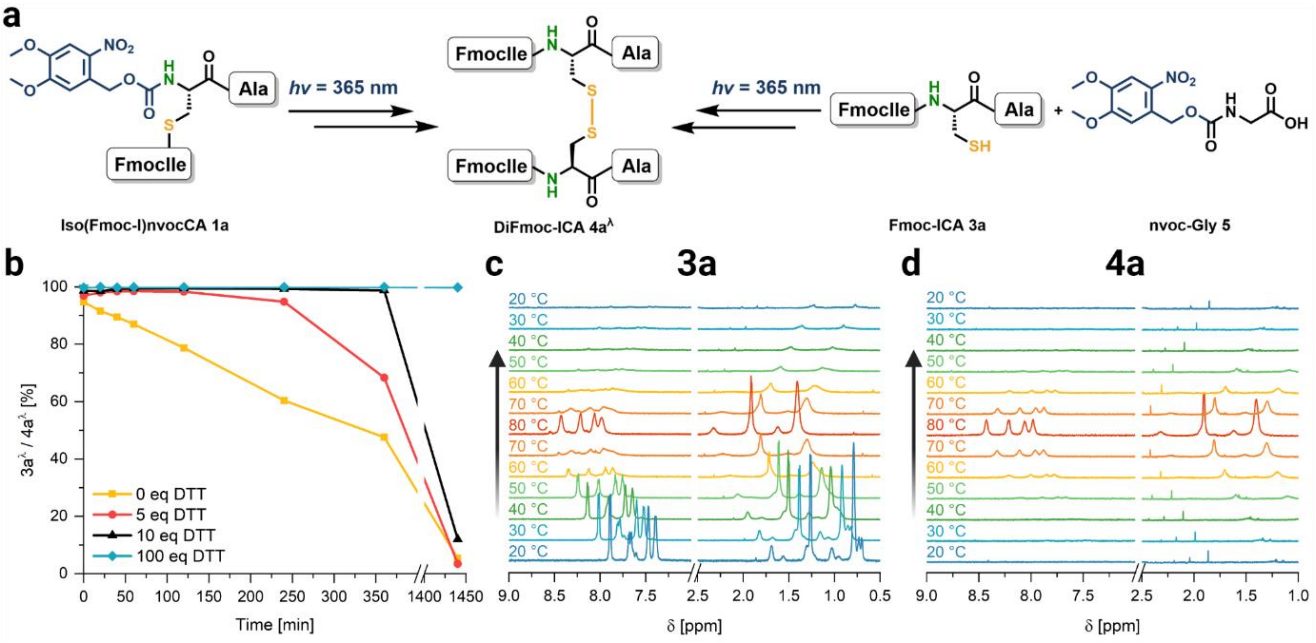

Figure 4: Tuneable oxidation by nvoc-Gly or DTT and the polymerization/depolymerization behaviour of 3a and 4a (NMR). (**a**) Control reaction of Fmoc-ICA **3a** with nvocGly leading to DiFmoc-ICA. (**b**) Ratio between **3a$^{\lambda}$** and **4a$^{\lambda}$** with different concentrations of DTT over 24 h. (**c**) Temperature dependent ^{1}H-NMR spectra of Fmoc-ICA **3a** over 3.5 h with the arrow indicating measurement sequence. (**d**) Temperature dependent ^{1}H-NMR spectra of DiFmoc-ICA **4a** over 3.5 h with an arrow indicating measurement sequence.

Nuclear magnetic resonance (NMR) and circular dichroism (CD) spectroscopy of **3a** and **4a** showed that both peptides possess different self-assembly kinetics and that the superstructures reveal unique thermal stabilities and depolymerisation kinetics. Upon temperature increase from 20 °C to 80 °C, ^{1}H NMR spectra of **3a** indicate an initial energy requirement for assembly where signal

broadening was observed upon heating to 70 °C (**Figure 4c**). Between 70–80 °C, the appearance of sharper resonances indicates a disassembly process of polymer **3a**, during which the monomer subunits are released into the bulk solvent. This depolymerisation process is further supported by diffusion ordered NMR (DOSY) (**SI Fig. 29, 30**). The cooling cycle back to 20 °C did not revert **3a** to its initial molecular state since the energy required to propagate assembly had already been met. To investigate whether an out-of-equilibrium state exists at the beginning of the temperature gradient, we analysed the assembly of **3a** over time at fixed temperatures of 20 °C and 60 °C with an internal standard (methylsulfonylmethane) to quantify the amount of non-assembled, free peptide (**Figure 5a**). At 20°C, it took 18 h to assemble 85% of **3a,** and this process was accelerated to 45 min at 60°C. This indicates that the self-assembly of **3a** is comparatively slow at room temperature but is greatly promoted at higher temperatures until 60 °C. Above 60 °C, depolymerisation processes become dominant, resulting in the reappearance of sharper resonances. In contrast, disulfide **4a** assembles rapidly at room temperature with thermal reversibility between 20 and 80 °C (**Figure 4d**). To probe the assembly mechanism, we seeded fragments of preformed **3a** and **4a**, each 10 mol%, into a monomer solution of **3a**. Neither the oxidised nor the reduced form of assembly nuclei showed a significant acceleration on the assembly process, suggesting an isodesmic (non-cooperative) assembly mechanism.

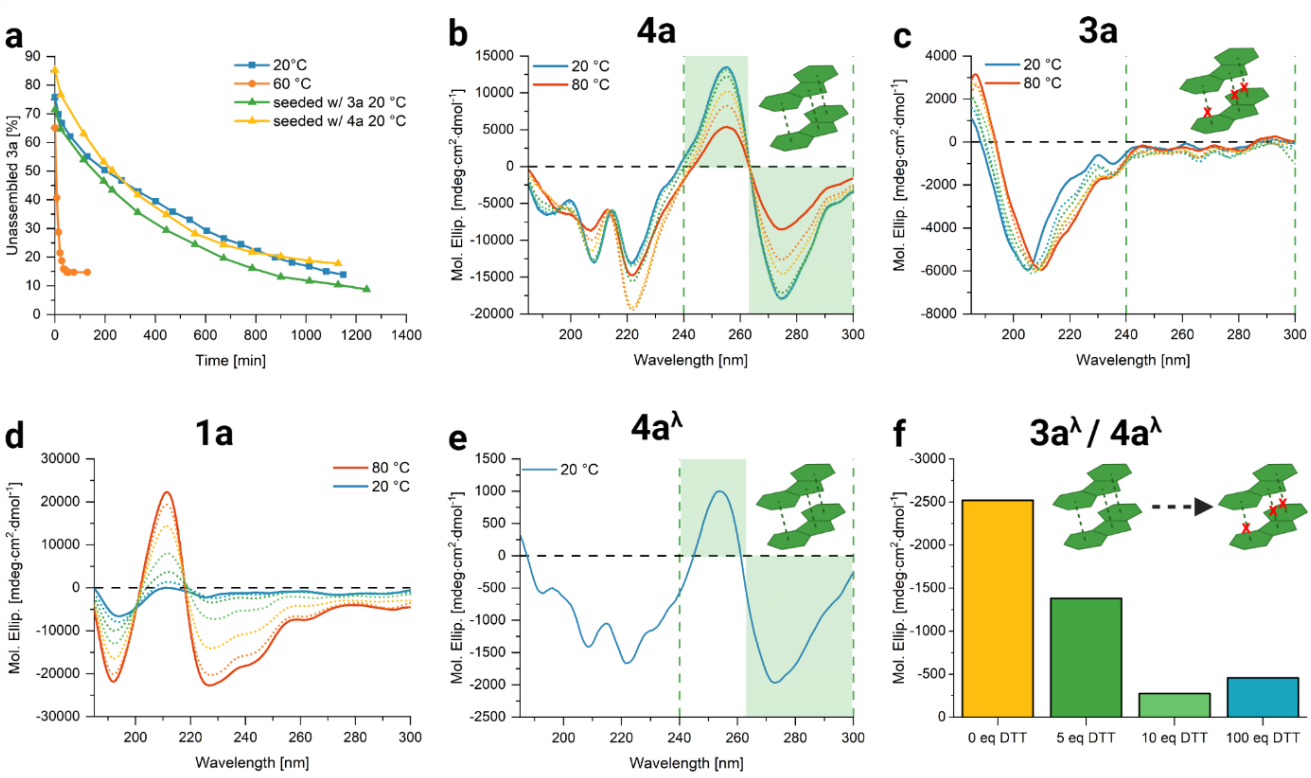

Figure 5: Temperature dependence of isodesmic assembly and secondary structure transformation of 3a and 4a. (**a**) Assembly kinetics calculated from the NMR spectra of the Fmoc-ICA monomer at 20 °C and 60 °C and seeding with **3a** and **4a** nanostructure fragments at 20 °C. (**b**) Temperature dependent CD spectra from 20–80 °C of DiFmoc-ICA **4a**, (**c**) Fmoc-ICA **3a**, (**d**) *iso*(Fmoc-I)nvocCA **1a** and (**e**) *iso*(Fmoc-I)nvocCA irradiated **4a**$^{\lambda}$ at 100 µM. (**f**) Molar ellipticity of **1a**$^{\lambda}$ with different DTT concentrations at 275 nm after 6 h.

CD analysis of **3a** and **4a** revealed major differences in the secondary structures of both assembled nanostructures. At 20 °C, **3a** shows a positive ellipticity at 185 nm and a negative Cotton effect at 204 nm attributed to the $n \rightarrow \pi^*$ transitions of the peptide backbone typical of a distorted α-helical structure (**Figure 5c**).[27] Increasing the temperature in 10 °C steps results in a bathochromic shift of the peaks, with the signals exhibiting full temperature reversibility (**SI Fig. 31**). Interesting, dimerization of **3a** to **4a** *via* the disulfide bond demonstrated a prominent change in the secondary structure of the assembly. Negative ellipticities at 191 nm, 208 nm, and 222 nm indicate an atypical twisted β-sheet structure (**Figure 5b**).[27] Additionally, the characteristic $\pi \rightarrow \pi^*$ transition of the Fmoc group at 255 nm, 275 nm, and 295 nm (green area) can only be found in the corresponding spectra of **4a**, indicating that the Fmoc group plays a critical role in the emergence of supramolecular chirality during the assembly process. Temperature cycling of **4a** showed further differences, where lower peak intensities instead of peak maxima were observed upon temperature increase. As a control, **1a**

alone is unstable upon heating (**Figure 5d**). After we have elucidated the supramolecular assembly characteristics of **3a** and **4a**, we then studied how the recycling cascade would direct the assembly landscape. Irradiation of **1a** leads to an assembly with a significant structural contribution of the Fmoc group (254 nm and 273 nm) and other signatures similar to that of **4a** (**Figure 5e**). This corroborates with the molecular analysis of the reaction cascade, during which **4a$^{\lambda}$** is formed quantitatively after 24 h upon the irradiation of **1a**. The same effect of DTT in extending the transience of **3a$^{\lambda}$** within the reaction cascade can be observed structurally by monitoring the differential between the Fmoc ellipticities of **3a$^{\lambda}$** and **4a$^{\lambda}$**. With increasing equivalents of DTT, the proportion of **3a$^{\lambda}$** increases, resulting in a decrease of the Fmoc contribution in the CD spectra at 275 nm (**Figure 5f**).

Given the major secondary structure differences between **3a** and **4a**, transmission electron microscopy (TEM) studies demonstrated associated contrasting features. The critical fibrillation concentrations of **3a** and **4a** in NH_4HCO_3 at pH 7.4 were found to be 50 µM and 10 µM respectively, indicating that the propensity for self-assembly is higher for the disulfide form (**SI Fig. 32, 33**). At 100 µM, in their native prepared state, unstructured nanofibres formed from **3a** and **4a** are found with fibre width of 12 ± 2 nm and 19 ± 3 nm, respectively (**SI Fig. 32, 33**). Subsequently, we used the same temperature gradients as for NMR and CD measurements (20°C - 80°C) for thermal annealing. Under these conditions, nanofibres exhibited higher order with **3a** adopting straight thin fibres with a diameter of 11 ± 3 nm (**Figure 6e**) whereas disulfide **4a** forms twisted fibres with a diameter of 12 ± 2 nm and a twist periodicity of 75 ± 7 nm (**Figure 6d**). Although thermal annealing processes are common in sample preparation to avoid trapped states during dissolution, the observed switch in morphology indicates that multiple levels of structural plasticity exist. By adapting such principles, , cells avoid erroneous assemblies and are able to switch between polymerization and depolymerisation processes quickly even under mild conditions.[20]

However, the assembly process and the structure it eventually adopt is dependent not only on the energy but also the availability of monomers at any given time. Hence, in the production of **4a$^{\lambda}$**, monomers are generated steadily as the oxidative photolysis takes place at room temperature. For **4a$^{\lambda}$**, it was observed that the twisted morphology of the fibres was formed without the need of thermal annealing (**Figure 6a**). This implies that the combined oxidation and assembly processes have circumvented trapped states and direct **4a$^{\lambda}$** to form the twisted nanostructures. To further substantiate that the recycling pathway of **4a$^{\lambda}$** produced nanofibres with identical surface chemistry to **4a**, we analyse the presence of sulfhydryl groups on the surface of the formed nanofibres using

Ellman's reagent. Quantification using cysteine as a standard revealed that both **4a$^{\lambda}$** and **4a** possess <5% sulfhydryl groups whereas **3a** showed a 91% availability (**Figure 6f**). In the absence of irradiation, the starting material **1a** does not form higher ordered architectures (**Figure 6c**). With the technology to elongate the transient time of **3a$^{\lambda}$** using DTT, visualization by TEM confirms that the features are similar to the model compound **3a** (**Figure 6b**). From the structural perspective, the reactions of **3a$^{\lambda}$** to form **4a$^{\lambda}$** and vice versa show how a disulfide bond propagates order and supramolecular chirality over structural hierarchies.

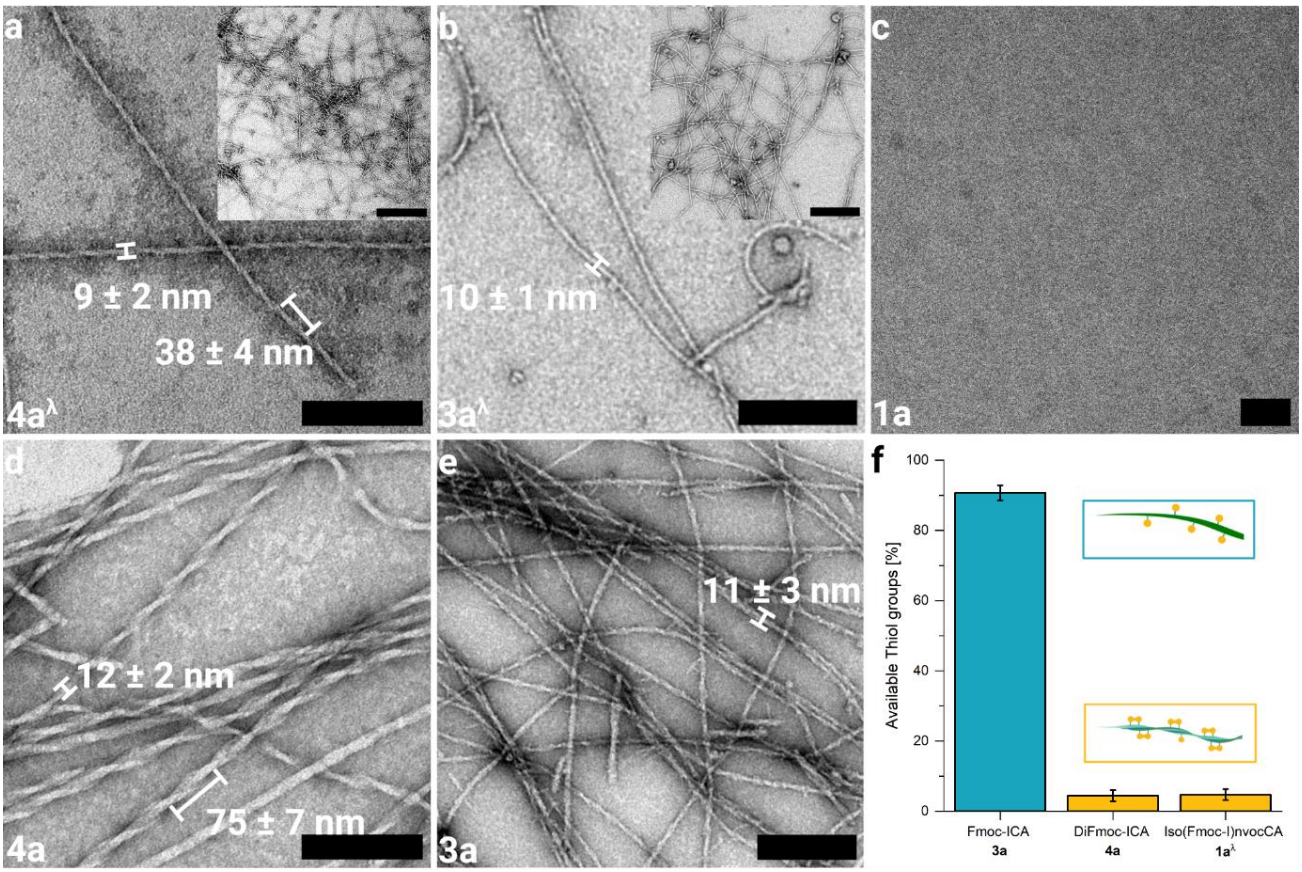

Figure 6: Differences in secondary structure of peptide fibres by TEM and oxidation state of fibres. (**a**) Peptide fibres of the irradiated *iso*-peptide **4a$^{\lambda}$**, (**b**) *iso*-peptide in the presence of 100 equiv. DTT **3a$^{\lambda}$**, (**c**) the non-irradiated *iso*-peptide **1a**, (**d**) DiFmoc-ICA **4a** after annealing and (**e**) Fmoc-ICA **3a** after annealing at 100 µM. TEM scalebars: 250 nm and 150 nm for **a** and **b** (big picture). (**f**) Quantification of available sulfhydryl groups on the fibre surface using Ellman's assay.

Conclusion

In conclusion, we have developed a recycling cascade that couples complex reaction dynamics to amplify nanostructure order and stability. Kinetic components of molecular transformation and supramolecular assembly of intermediates describe their interplay within the global redox environment. An increase in structural order and supramolecular chirality of **4a$^{\lambda}$** emerges as a consequence of the multistep cascade due to the continuous formation of the active assembly monomer, which would otherwise require thermal intervention. The disulfide bond alters the aromatic contribution of the monomer, impacting the secondary structure of the fibrils and discriminates **3a$^{\lambda}$** from **4a$^{\lambda}$**. By controlling the redox balance between $N{=}O_{nitroso}$ and DTT, the transience of **3a$^{\lambda}$** can be lengthened thus delaying the production of **4a$^{\lambda}$**. The presented approach encompasses a number of strategies adopted in nature to recycle chemical energy and propagate higher order in hierarchical structures through the controlled and reversible production of assembly intermediates. Based on one type of monomer, supramolecular polymers with structural plasticity and multiple structural states were obtained, an important feature otherwise mainly observed in actin filaments and microtubules. We believe that the presented integrative chemical concept provides a fresh perspective on the bottom-up synthesis of nanostructures and greatly expands the repertoire of dynamic supramolecular architectures that can be formed under mild conditions.

Acknowledgements

The authors gratefully acknowledge financial support from the Max Planck-Bristol Centre for Minimal Biology.

Data Availability

The data that support the findings of this study are available in the supporting information and from the corresponding authors upon reasonable request.

Author contributions

P.R., D.Y.W.N., and T.W. conceived the project. P.R. and R.M. performed the synthesis experiments and kinetics. P.R. conducted TEM and CD analysis. R.M. and M.W. performed the NMR analysis. R.M. conducted the Ellman's assay. P.R., R.M., D.Y.W.N. and T.W. wrote the manuscript. D.Y.W.N. and T.W. supervised the project. All authors have read and approved the final manuscript.

References

1. Bassham, J. A. & Calvin, M. The path of carbon in photosynthesis. in *Die CO2-Assimilation / The*

Assimilation of Carbon Dioxide 884–922 (Springer Berlin Heidelberg, 1960). doi:10.1007/978-3-642-94798-8_30.
2. Barber, J. & Andersson, B. Revealing the blueprint of photosynthesis. *Nature* **370**, 31–34 (1994).
3. Conibear, E. & Tam, Y. Y. C. The Endocytic Pathway. *Traffick. Insid. Cells* **2**, 67–83 (2009).
4. Kornberg, H. L. & Krebs, H. A. Synthesis of cell constituents from C2-units by a modified tricarboxylic acid cycle. *Nature* **179**, 988–991 (1957).
5. Krebs, H. The history of the tricarboxylic acid cycle of the pathways of anaerobic energy metabolism. *Perspect. Biol. Med.* **14**, 154–72 (1970).
6. Dogterom, M. & Koenderink, G. H. Actin–microtubule crosstalk in cell biology. *Nat. Rev. Mol. Cell Biol.* **20**, 38–54 (2019).
7. Boekhoven, J., Hendriksen, W. E., Koper, G. J. M., Eelkema, R. & van Esch, J. H. Transient assembly of active materials fueled by a chemical reaction. *Science.* **349**, 1075–1079 (2015).
8. Karsenti, E. Self-organization in cell biology: a brief history. *Nat. Rev. Mol. Cell Biol.* **9**, 255–262 (2008).
9. Nédélec, F. J., Surrey, T., Maggs, A. C. & Leibler, S. Self-organization of microtubules and motors. *Nature* **389**, 305–308 (1997).
10. Aida, T., Meijer, E. W. & Stupp, S. I. Functional supramolecular polymers. *Science.* **335**, 813–817 (2012).
11. Schnitzer, T., Jansen, S. A. H., Mabesoone, M. F. J., Vantomme, G. & Meijer, E. W. In situ Synthesis of Supramolecular Polymers: Finding the Right Conditions when Combining Covalent and Non-Covalent Synthesis. *Angew. Chemie Int. Ed.* **202206729**, (2022).
12. Rieß, B., Grötsch, R. K. & Boekhoven, J. The Design of Dissipative Molecular Assemblies Driven by Chemical Reaction Cycles. *Chem* **6**, 552–578 (2020).
13. Chen, Z. *et al.* Solvent-free autocatalytic supramolecular polymerization. *Nat. Mater.* **21**, 253–261 (2022).
14. Chakraborty, P. *et al.* Nanoengineered Peptide-Based Antimicrobial Conductive Supramolecular Biomaterial for Cardiac Tissue Engineering. *Adv. Mater.* **2008715**, 1–10 (2021).
15. Álvarez, Z. *et al.* Bioactive scaffolds with enhanced supramolecular motion promote recovery from spinal cord injury. *Science.* **374**, 848–856 (2021).
16. Yang, S. *et al.* Chemical Fueling Enables Molecular Complexification of Self-Replicators**. *Angew. Chemie - Int. Ed.* **60**, 11344–11349 (2021).
17. Mattia, E. & Otto, S. Supramolecular systems chemistry. *Nat. Nanotechnol.* **10**, 111–119 (2015).
18. Leira-Iglesias, J., Tassoni, A., Adachi, T., Stich, M. & Hermans, T. M. Oscillations, travelling fronts and patterns in a supramolecular system. *Nat. Nanotechnol.* **13**, 1021–1027 (2018).
19. Maiti, S., Fortunati, I., Ferrante, C., Scrimin, P. & Prins, L. J. Dissipative self-assembly of vesicular nanoreactors. *Nat. Chem.* **8**, 725–731 (2016).
20. Kueh, H. Y. & Mitchison, T. J. Structural Plasticity in Actin and Tubulin Polymer Dynamics. *Science.* **325**, 960–963 (2009).
21. Steinmetz, M. O., Goldie, K. N. & Aebi, U. A correlative analysis of actin filament assembly, structure, and dynamics. *J. Cell Biol.* **138**, 559–574 (1997).
22. Molodtsov, M. I., Grishchuk, E. L., Efremov, A. K., McIntosh, J. R. & Ataullakhanov, F. I. Force production by depolymerizing microtubules: A theoretical study. *Proc. Natl. Acad. Sci. U. S. A.* **102**, 4353–4358 (2005).
23. Xue, Y. *et al.* Stimulus-cleavable chemistry in the field of controlled drug delivery. *Chem. Soc. Rev.* **50**, 4872–4931 (2021).

24. Klán, P. *et al.* Photoremovable protecting groups in chemistry and biology: Reaction mechanisms and efficacy. *Chem. Rev.* **113**, 119–191 (2013).
25. Ellis, M. K., Hill, S. & Foster, P. M. D. Reactions of nitrosonitrobenzenes with biological thiols: Identification and reactivity of glutathion-S-yl conjugates. *Chem. Biol. Interact.* **82**, 151–163 (1992).
26. Pieszka, M. *et al.* Controlled Supramolecular Assembly Inside Living Cells by Sequential Multistaged Chemical Reactions. *J. Am. Chem. Soc.* **142**, 15780–15789 (2020).
27. Xing, Q. *et al.* Aromatic Motifs Dictate Nanohelix Handedness of Tripeptides. *ACS Nano* **12**, 12305–12314 (2018).